A MPFA METHOD USING HARMONIC POINTS COUPLED TO A MULTIDIMENSIONAL OPTIMAL ORDER DETECTION METHOD (MOOD) FOR THE SIMULATION OF OIL-WATER DISPLACEMENTS IN PETROLEUM RESERVOIRS

[1]Contreras Fernando RL

[2]Souza Marcio RA

ferlicapac@gmail.com

souza2105@gmail.com

[3]Lyra Paulo RM

[4]Carvalho Darlan KE

prmlyra@padmec.org

dkarlo@oul.com.br

[1,3,4]*Departmento de Engenharia Mecânica, UFPE,* Av. Acadêmico Hélio Ramos s/n, CEP: 50670-901, Pernambuco, Recife, Brazil.. [2]*Departmento de Engenharia Energia Renovable, UFPB,* BR 230, km 21 s/n, CEP: 58059-900, João Pessoa, PB, Brazil

Abstract. In this paper, our main goal is to present a non-classical MPFA method coupled with a high order finite volume method for the simulation of oil water displacements in heterogeneous and anisotropic petroleum reservoirs using general polygonal meshes. The governing equations are solved using the IMPES (IMplicit Pressure and Explicit Saturation) strategy, where the elliptic pressure equation is discretized by a linear Multipoint Flux Approximation method using Harmonic points (MPFA-H) capable to handle strongly heterogeneous and anisotropic media. Besides, to approximate the advective term that characterizes the hyperbolic saturation equation, we use the Multidimensional Optimal Order Detection (MOOD) method. This technique is based in an "a posteriori" limitation procedure, i.e., the limitation procedure is done after the calculation of "candidate solutions" only where necessary to guarantee certain physical properties such as monotonicity. To show the potential of our finite volume formulation, we solve some benchmark problems found in literature.

Keywords: Numerical simulation, Oil and Water displacements, Heterogeneous and anisotropic porous media, MPFA-H, MOOD.

1   INTRODUCTION

The numerical simulation of fluid flow in highly heterogeneous and anisotropic oil and gas reservoirs pose a great challenge for numerical algorithms, due to the modeling of complex depositional environments, including inclined laminated layers, channels, fractures and faults and the modeling of deviated wells that have profound effects on the flow inside the reservoirs. The development and application of a particular locally conservative numerical algorithm able to deal with some of these challenges is the subject of the present paper.

Under certain simplifying assumptions, the basic equations that describe flow through porous media can be expressed in terms of two coupled equations, an elliptic type pressure equation with a heterogeneous and eventually highly discontinuous permeability coefficient for the pressure field and a non-linear hyperbolic equation for the saturation field. Commonly, in commercial simulators, the elliptic term associated to the pressure discretization is approximated by a simple Two Point Flux Approximation (TPFA) method and the hyperbolic term associated to the saturation discretization is approximated via a simple First Order Upwind (FOU) method (Bell and Shubin 1985; Durlofsky 1993; Edwards 1996; Edwards 2006; Contreras et al., 2016). Even though this combined strategy is simple to implement and highly computationally efficient, it has certain drawbacks related to the inability of the TPFA method to properly discretize complex geometries that associated to the geological modeling of the faulted and inclined structure of the reservoir and the anisotropic numerical diffusion introduced by the FOU method, which, not only, generates excessive numerical spreading of the saturation fronts but that is also prone to the so called Grid Orientation Effect (GOE) which represents a strong dependence of the numerical solution on the orientation of grid lines (Kozdon et al., 2011; Contreras et al., 2016). The consequence of these drawbacks are erroneous predictions of breakthrough times and the dissipation of fluid banks to the point that miscibility effects are incorrectly predicted (Bell and Shubin 1985).

In this context, in the present paper we devise a full cell-centered finite volume procedure to solve both, the pressure and the saturation equations, via an IMplicit Pressure-Explicit Satura-tion (IMPES) technique which was originally devised by Sheldon and Cardwell (1959) and Stone and Gardner (1961) and has been extensively used in practice for moderate complexity multiphase flow problems in petroleum reservoirs. The pressure equation is discretized by a non-orthodox cell-centered Multipoint Flux Approximation Method using harmonic point (MPFA-H), this linear method was based on classical non-linear methods (Le Potier 2005; Lipnikov et al., 2007; Yuan and Sheng 2008) to solve diffusion problems in strongly heterogeneous and anisotropic media using polygonal meshes. Using some of the basic ideas of Non-Linear Finite Volume methods, in our linear MPFA-H formulation, we first construct the one sided fluxes on each control surface independently and then a unique flux expression is obtained by a convex combination of the one sided fluxes. Differently from other classical MPFA methods, in this scheme, fluxes on each cell face are explicitly expressed by one cell centered unknown and points defined on the faces that do not necessarily belong to the same face shared by the adjacent cells. These auxiliary points are calculated from the harmonic points concept (Agelas et al., 2009).

To solve the non-linear saturation equation with improved accuracy different strategies are proposed. The MUSCL (Monotone Upstream Centered Scheme for Conservation Laws) method of van Leer (1979) is usually used to numerically solve the saturation equation (Bell and Shubin 1985; Durlofsky 1993; Edwards 1996; Edwards 2006; Contreras et al., 2016). In this method, second order accuracy is obtained by a local linear reconstruction process, and local extrema associated to strong solution gradients are eliminated by an *"a priori"*

limitation procedure. This method can be adapted for unstructured meshes in a very robust way (Woodfield et al., 2014; Contreras et al., 2016).

In this article, we adapt a novel method proposed by (Clain et al., 2011) called Multidimensional Optimal Order Detection (MOOD), which was originally developed for classical hydrodynamics applications. This scheme is radically different from traditional high order methods, since it is based on an *"a posteriori"* limitation procedure. In short, the MOOD scheme consists in to determine an optimal polynomial degree reconstruction for each control volume (CV) at each time step, satisfying some physical restriction, e.g., monotonicity. Then, the candidate solution in all control volumes is rigorously analyzed by the physical criteria. Whenever the physical criteria are violated in the control volume, the latter is marked as a "bad CV" and this solution is automatically discarded and the decree of the polynomial is decreased until the physical restriction is satisfied in the CV. This high resolution scheme is relatively simple, very efficient and accurate, producing solutions that are multidimensional in nature, being very competitive with others found in literature.

In order to validate our formulation, i.e., the use the proposed MPFA-H method for the pressure field, combined with the Multidimensional Optimal Order Degree (MOOD) for the saturation one, we simulate oil–water displacements with moderate or high mobility ratios, in heterogeneous and anisotropic (full tensor) oil reservoirs using structured and unstructured triangular and quadrilateral meshes.

2   MATHEMATICAL FORMULATION

In this section, we briefly describe the governing equations for the two-phase flow of oil and water in petroleum reservoirs. We assume, without loss of generality, that the fluid and rock are both incompressible, that the flow is isothermal and we neglect the capillary pressure. We will use a segregated formulation in which the basic equations are obtained from the adequate combination of the conservation of mass and the Darcy's Law, which can be written for phases *i =o (oil), w (water)*, respectively, as:

$$\frac{\partial(\phi\rho_i S_i)}{\partial t} = -\nabla \cdot (\rho_i \vec{v}_i) + q_i \tag{1}$$

and

$$\vec{v}_i = -\lambda_i \underset{\sim}{K} \nabla p_i, \ i = o, w \tag{2}$$

In Equations (1) and (2), ϕ is the rock porosity, ρ_i and S_i, represent, the density and the saturation of phase *i*, i.e., the fraction of the pore volume occupied by phase *i*, respectively. $\vec{v}_i$ is the phase velocity, which is given by Darcy's law and q_i denotes source or sink terms (e.g., injection or production wells) and $\underset{\sim}{K}$ is the absolute rock permeability tensor that satisfies the ellipticity condition and the fluid mobility is given by $\lambda_i = k_{ri}/\mu_i$, where μ_i and $k_{ri}(S_i)$ represent the viscosity and the relative permeability of phase *i*, respectively. We also assume that the reservoir rock is fully saturated by oil and water. Due to this last assumption, we can write:

$$S_o + S_w = 1 \tag{3}$$

By using equations (1) to (3) and after some algebraic manipulation (Ewing 1983, Peaceman 1977), we can write the elliptic pressure equation, as:

$$\nabla \cdot \vec{v} = Q \quad \text{with} \quad \vec{v} = -\lambda \underset{\sim}{K} \nabla p \tag{4}$$

In previous equation the total mobility is denoted by $\lambda = \lambda_w + \lambda_o$. The total fluid velocity is denoted by $\vec{v} = \vec{v}_w + \vec{v}_o$ and the total fluid injection or production specific rate is denoted by $Q = Q_w + Q_o$ with $Q_i = q_i / \rho_i$. Again, by using equations (1) to (3) and after some algebraic manipulation, we can write the hyperbolic saturation equation, as:

$$\phi \frac{\partial S_w}{\partial t} = -\nabla \cdot \vec{F}(S_w) + Q_w \tag{5}$$

In Equation (5), the flux function is defined by $\vec{F}(S_w) = f_w \vec{v}$ where $f_w = \lambda_w / \lambda$ is the fractional flow of water, which is a non-linear function of the water-phase saturation. Equation (5) is a non-linear hyperbolic equation from which discontinuous profiles can evolve even from smooth initial solutions (Ewing 1983).

2.1   2.1 Initial and boundary conditions

The problem described by Equations (4) and (5) is only completely determined when we use an appropriate set of initial and boundary conditions. Typical boundary and initial conditions are given by (Carvalho et al., 2007; Contreras et al., 2016):

$$
\begin{aligned}
p(\vec{x}, t) &= g_D & on & \quad \Gamma_D \times [0, t], \\
\vec{v} \cdot \vec{n} &= g_N & on & \quad \Gamma_N \times [0, t], \\
S_w(\vec{x}, t) &= \overline{S}_w & on & \quad \Gamma_I \times [0, t], \\
S_w(\vec{x}, 0) &= \overline{S}_w^0 & on & \quad \Omega
\end{aligned}
\tag{6}
$$

where Γ_D, Γ_N represent the Dirichlet and Neumann boundaries, respectively, and Γ_I represents injection wells. The scalar function g_D (prescribed pressures) is defined in Γ_D and g_N (prescribed fluxes) is defined in Γ_N, $\overline{S}_w$ represents the saturation prescribed in a set of injection wells and finally, $\overline{S}_w^0$ is the initial saturation distribution.

3   NUMERICAL FORMULATION

As previously mentioned, the pressure and the saturation equations are sequentially solved in an IMPES segragated procedure. In this formulation, given an initial distribution of saturation of fluids within the reservoir, we calculate the pressure unknown implicitly, then we compute the flow field which is used as an input for the explicit computation of the saturation unknown. The process repeats until the end of the simulation. The main advantages of the IMPES methodology are its simplicity of implementation and its low computational

cost for each time step, even though, depending on the complexity problem, the time step restriction associated to the CFL condition may be too severe, turning this method impractical for some practical applications.

3.1 Implicit formulation for the pressure equation by the MPFA-H method

The discretization of the continuous domain is performed by an open set polygonal $\Omega \subset R^2$ with boundary denoted by $\partial\Omega = \bar{\Omega} \setminus \Omega$ (the closure of Ω is denoted by $\bar{\Omega}$). An admissible discretization involves the composition of three supersets denoted by $\mathcal{D} = (\mathcal{M}, \mathcal{E}, O)$, where:

• $\mathcal{M} = \{\hat{L}\}$ is a finite family of control volumes such that: $\bigcup_{\hat{L} \in \mathcal{M}} \bar{L} = \bar{\Omega}$, where each control volume is considered a star-shaped polygonal with respect to the barycenter. The volume (area in 2D) of $\hat{L} \in \mathcal{M}$ is denoted by $V_{\hat{L}}$ and the cardinality of $\mathcal{M}$ is given by n.

• $\mathcal{E} = \{IJ\}$ is a finite family of edges in $\bar{\Omega}$, usually called control surfaces. For each $\hat{L} \in \mathcal{M}$, there exist a subset $\mathcal{E}_{\hat{L}}$ of $\mathcal{E}$ such that: $\bigcup_{IJ \in \mathcal{E}_{\hat{L}}} \overline{IJ} = \partial\hat{L}$. Also, we assume that for all $IJ \in \mathcal{E}$, we have $IJ \subset \partial\Omega$ or $IJ \subseteq \hat{L} \cap \hat{R}$, for some $(\hat{L}, \hat{R}) \in \mathcal{M} \times \mathcal{M}$. The set of internal and external edges are denoted, respectively by $\mathcal{E}^{\text{int}} = \mathcal{E} \cap \Omega$ and $\mathcal{E}^{ext} = \mathcal{E} \cap \partial\Omega$. Finally, the length of the edge IJ is given by the Euclidean norm $\|\overline{IJ}\|$.

• $O = \{x_{\hat{L}}\}_{\hat{L} \in \mathcal{M}}$ is a finite family of points (barycenters of the control volumes) of Ω, so that, for all $\hat{L} \in \mathcal{M}$, $x_{\hat{L}} \in \hat{L}$.

After describing the components that define the discrete domain, we proceed to integrate the pressure equation (4) over a control volume $\hat{L} \in \mathcal{M}$ and by applying the Gauss divergence theorem, it can be written as:

$$\int_{\partial\hat{L}} \vec{v} \cdot \vec{n} \, ds = \int_{\hat{L}} Q dV \tag{7}$$

where $\vec{n}$ denotes the unit outward normal vector to $\partial\hat{L}$.

Therefore, the left and right sides of equation (7) can be approximated, respectively, as follow:

$$\int_{\partial\hat{L}} \vec{v} \cdot \vec{n} \, ds \cong \sum_{IJ \in \mathcal{E}_{\hat{L}}} \vec{v}_{IJ} \cdot \vec{N}_{IJ}, \quad \int_{\hat{L}} Q dV \cong \bar{Q}_{\hat{L}} V_{\hat{L}} \quad \text{and} \quad \vec{v}_{IJ} = \frac{1}{\|\overline{IJ}\|} \int_{IJ} \vec{v} \, ds \tag{8}$$

This scheme is locally conservative because satisfies the following equation:

$$\vec{v}_{IJ} \cdot \vec{N}_{IJ} + \vec{v}_{IJ} \cdot \vec{N}_{JI} = 0 \tag{9}$$

In Equation (4) the mid-edge mobility λ_{IJ} is obtained by using the arithmetic average of the nodal mobilities and the volume averaged nodal mobilities are given by:

$$\lambda_j = \sum_{\hat{L}=1}^{n_j} \lambda_{\hat{L}} V_{\hat{L}} \Big/ \sum_{\hat{L}=1}^{n_j} V_{\hat{L}}, \quad j = I, J \tag{10}$$

Here, $\lambda_{\hat{L}}$ is the total mobility of each control volume surrounding node j and n_j is the number of control volumes surrounding node j.

In Equation (8), the numerical flow $\vec{v}_{IJ} \cdot \vec{N}_{IJ}$ can be approximated in many ways, each one leading to a different linear or non-linear finite volume schemes (Edwards et al., 1998; Aavatsmark et al., 2002, Le Potier, 2005; Lipnikov et al., 2007; Yuan and Sheng 2008; Gao and Wu 2010).

From equation (4) and (7), the one sided flux with respect control volume $\hat{L}$, is expressed as:

$$\int_{IJ} \vec{v} \cdot \vec{n}_{IJ} \mathrm{d}s = -\int_{IJ} \lambda \underset{\sim}{K}_{\hat{L}} \nabla p \cdot \vec{n}_{IJ} \mathrm{d}s = -\int_{IJ} \lambda \nabla p \cdot \underset{\sim}{K}_{\hat{L}}^{\mathsf{T}} \vec{n}_{IJ} \mathrm{d}s, \; IJ \in \mathscr{E}_{\hat{L}} \tag{11}$$

where $\underset{\sim}{K}_{\hat{L}}^{\mathsf{T}}$ represent the matrix transpose of $\underset{\sim}{K}_{\hat{L}}$. In the previous equation we need to approximate the term $\nabla p \cdot \underset{\sim}{K}_{\hat{L}}^{\mathsf{T}} \vec{n}_{IJ}$, using the Taylor series expansion (Yuan and Sheng 2008).

Since that $\overrightarrow{x_{\hat{L}} x_{\hat{L},i(IJ)}}$ and $\overrightarrow{x_{\hat{L}} x_{\hat{L},j(IJ)}}$ are edges of the triangle $\Delta x_{\hat{L}} x_{\hat{L},i(IJ)} x_{\hat{L},j(IJ)}$, the term $\underset{\sim}{K}_{\hat{L}}^{\mathsf{T}} \cdot \vec{n}_{IJ}$ can be writen as a linear combination of those edges as

$$\underset{\sim}{K}_{\hat{L}}^{\mathsf{T}} \vec{n}_{IJ} = \alpha_{\hat{L},i(IJ)} \overrightarrow{x_{\hat{L}} x_{\hat{L},i(IJ)}} + \alpha_{\hat{L},j(IJ)} \overrightarrow{x_{\hat{L}} x_{\hat{L},j(IJ)}} \tag{12}$$

where $x_{\hat{L},i(IJ)}$ and $x_{\hat{L},j(IJ)}$ are the interpolation points showed in Fig. 1. The coefficients $\alpha_{\hat{L},i(IJ)}$ and $\alpha_{\hat{L},j(IJ)}$ are given by:

$$\alpha_{\hat{L},i(IJ)} = \frac{\left\| \underset{\sim}{K}_{\hat{L}}^{\mathsf{T}} \vec{n}_{IJ} \right\| \sin(\theta_{\hat{L},IJ}^1)}{\sin(\theta_{\hat{L},IJ}^1 + \theta_{\hat{L},IJ}^2)} \; \text{ and } \; \alpha_{\hat{L},j(IJ)} = \frac{\left\| \underset{\sim}{K}_{\hat{L}}^{\mathsf{T}} \vec{n}_{IJ} \right\| \sin(\theta_{\hat{L},IJ}^2)}{\sin(\theta_{\hat{L},IJ}^1 + \theta_{\hat{L},IJ}^2)} \tag{13}$$

In the previous equation the coefficients exist and are non-negative when the angles formed by segments $\overrightarrow{x_{\hat{L}} x_{\hat{L},i(IJ)}}$ (resp. $\overrightarrow{x_{\hat{L}} x_{\hat{L},j(IJ)}}$) and the co-normal $\underset{\sim}{K}_{\hat{L}}^{\mathsf{T}} \vec{n}_{IJ}$, satisfies the following conditions $0 < \theta_{\hat{L},IJ}^1, \theta_{\hat{L},IJ}^2 < \pi$ and $\theta_{\hat{L},IJ}^1 + \theta_{\hat{L},IJ}^2 < \pi$. The non-negative coefficients is essential in non-linear methods to assure the monotone or extremum-preserving properties (Le Potier 2005; Lipnikov et al., 2007; Yuan and Sheng 2008; Gao and Wu 2013).

We can proceed to substitute the equation (12) into equation(11), obtaining the following equation

$$\int_{IJ} -\lambda \underset{\sim}{K} \nabla p \cdot \vec{n}_{IJ} \mathrm{d}s = -\int_{IJ} \lambda \left(\alpha_{\hat{L},i(IJ)} \nabla p \cdot \overrightarrow{x_{\hat{L}} x_{\hat{L},i(IJ)}} + \alpha_{\hat{L},j(IJ)} \nabla p \cdot \overrightarrow{x_{\hat{L},j(IJ)} x_{\hat{L}}} \right) \mathrm{d}s \tag{14}$$
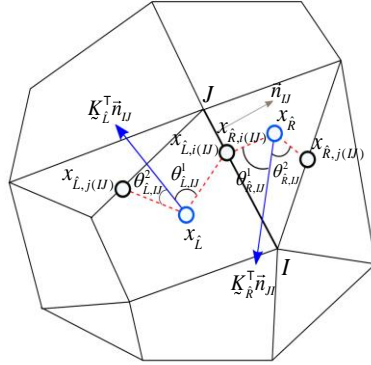
Figure 1. Representation of the physical and geometric parameters for the MPFA-H method.

We use a local finite difference method to approximate the partial derivatives ∇p along directions $\overrightarrow{x_{\hat{L},j(IJ)} x_{\hat{L}}}$ and $\overrightarrow{x_{\hat{L}} x_{\hat{L},i(IJ)}}$ (Yuan and Sheng 2008):

$$\int_{IJ} -\lambda \underset{\sim}{K} \nabla p \cdot \vec{n}_{IJ} \mathrm{d}s = -\lambda_{IJ} \left\| \overrightarrow{IJ} \right\| \left(\alpha_{\hat{L},i(IJ)} \frac{p_{\hat{L},i(IJ)} - p_{\hat{L}}}{\left\| \overrightarrow{x_{\hat{L}} x_{\hat{L},i(IJ)}} \right\|} + \alpha_{\hat{L},j(IJ)} \frac{p_{\hat{L},j(IJ)} - p_{\hat{L}}}{\left\| \overrightarrow{x_{\hat{L}} x_{\hat{L},j(IJ)}} \right\|} \right) \text{ and } \lambda_{IJ} \left\| \overrightarrow{IJ} \right\| = \int_{IJ} \lambda \mathrm{d}s \tag{15}$$

Equation (15) is equivalent to

$$\vec{v}_{IJ}^{\hat{L}} \cdot \vec{N}_{IJ} = \lambda_{IJ} \left\| \overrightarrow{IJ} \right\| \left(\xi_{\hat{L},i(IJ)} \left(p_{\hat{L}} - p_{\hat{L},i(IJ)} \right) + \xi_{\hat{L},j(IJ)} \left(p_{\hat{L}} - p_{\hat{L},j(IJ)} \right) \right) \tag{16}$$

where

$$\xi_{\hat{L},i(IJ)} = \frac{\alpha_{\hat{L},i(IJ)}}{\left\| \overrightarrow{x_{\hat{L}} x_{\hat{L},i(IJ)}} \right\|} \text{ and } \xi_{\hat{L},j(IJ)} = \frac{\alpha_{\hat{L},j(IJ)}}{\left\| \overrightarrow{x_{\hat{L}} x_{\hat{L},j(IJ)}} \right\|} \tag{17}$$

Similarly, we can write the one sided flux respect to a control volume $\hat{R}$, as:

$$\vec{v}_{IJ}^{\hat{R}} \cdot \vec{N}_{JI} = \lambda_{IJ} \left\| \overrightarrow{IJ} \right\| \left(\xi_{\hat{R},i(IJ)} \left(p_{\hat{R}} - p_{\hat{R},i(IJ)} \right) + \xi_{\hat{R},j(IJ)} \left(p_{\hat{R}} - p_{\hat{R},j(IJ)} \right) \right) \tag{18}$$

where $x_{\hat{R},i(IJ)}$, $x_{\hat{R},j(IJ)}$ are the interpolation points with respect to control volume $\hat{R}$ (see Fig. 1) and the coefficients are given by:

$$\xi_{\hat{R},i(IJ)} = \frac{\alpha_{\hat{R},i(IJ)}}{\left\| \overrightarrow{x_{\hat{R}} x_{\hat{R},i(IJ)}} \right\|} \text{ and } \xi_{\hat{R},j(IJ)} = \frac{\alpha_{\hat{R},j(IJ)}}{\left\| \overrightarrow{x_{\hat{R}} x_{\hat{R},j(IJ)}} \right\|} \tag{19}$$

3.2   Construction of the unique flux.

In order to construct a conservative scheme, we use the one side fluxes defined in equations (16) and (18) to define the unique flux on the face (*IJ*) (Fuhrmann et al., 2014), therefore

$$\vec{v}_{IJ} \cdot \vec{N}_{IJ} = w_{\hat{R},IJ} \vec{v}_{IJ}^{\hat{L}} \cdot \vec{N}_{IJ} - w_{\hat{L},IJ} \vec{v}_{IJ}^{\hat{R}} \cdot \vec{N}_{JI} \tag{20}$$

where the weights $w_{\hat{L},IJ}$, $w_{\hat{R},IJ}$ are defined as

$$w_{\hat{L},IJ} = \frac{h_{\hat{R},IJ} k_{\hat{L},IJ}^{(n)}}{h_{\hat{L},IJ} k_{\hat{R},IJ}^{(n)} + h_{\hat{R},IJ} k_{\hat{L},IJ}^{(n)}} \quad \text{and} \quad w_{\hat{R},IJ} = 1 - w_{\hat{L},IJ} \tag{21}$$

The projections of the permeability tensor of the adjacent control volumes that share edge *IJ* on the normal directions to this edge is denoted by $k_{\hat{L},IJ}^{(n)} = \vec{n}_{IJ}^{\mathsf{T}} \underset{\sim}{K}_{\hat{L}} \vec{n}_{IJ}$ and $k_{\hat{R},IJ}^{(n)} = \vec{n}_{IJ}^{\mathsf{T}} \underset{\sim}{K}_{\hat{R}} \vec{n}_{IJ}$, and the orthogonal distance from $x_{\hat{L}}$ (resp. $x_{\hat{R}}$) on *IJ* is denoted by $h_{\hat{L},IJ}$ (resp. $h_{\hat{R},IJ}$). Note that the weight in previous equation satisfying the restriction condition $w_{\hat{L},IJ} + w_{\hat{R},IJ} = 1$ (Le Potier, 2005; Lipnikov et al., 2007; Yuan and Sheng 2008). The fluxes given in the equations (16) and (18) are introduced into equation (20), and after some algebraic manipulation, we have:

$$\vec{v}_{IJ} \cdot \vec{N}_{IJ} = \lambda_{IJ} \left\| \overline{IJ} \right\| \left(\kappa_{\hat{L},IJ} p_{\hat{L}} - \kappa_{\hat{R},IJ} p_{\hat{R}} + \sum_{\gamma=i,j} \left(G_{\hat{R},\gamma(IJ)} p_{\hat{R},\gamma(IJ)} - G_{\hat{L},\gamma(IJ)} p_{\hat{L},\gamma(IJ)} \right) \right) \tag{22}$$

where

$$\kappa_{\hat{L},IJ} = w_{\hat{L},IJ} \left(\xi_{\hat{L},i(IJ)} + \xi_{\hat{L},j(IJ)} \right), \quad \kappa_{\hat{R},IJ} = w_{\hat{R},IJ} \left(\xi_{\hat{R},i(IJ)} + \xi_{\hat{R},j(IJ)} \right), \tag{23}$$

$$G_{\hat{L},\gamma(IJ)} = w_{\hat{L},IJ} \xi_{\hat{L},\gamma(IJ)} \quad \text{and} \quad G_{\hat{R},\gamma(IJ)} = w_{\hat{R},IJ} \xi_{\hat{R},\gamma(IJ)}, \quad \gamma = i, j \tag{24}$$

Is similar for the control volume $\hat{R}$:

$$\vec{v}_{IJ} \cdot \vec{N}_{JI} = \lambda_{IJ} \left\| \overline{IJ} \right\| \left(\kappa_{\hat{R},IJ} p_{\hat{R}} - \kappa_{\hat{L},IJ} p_{\hat{L}} + \sum_{\gamma=i,j} \left(G_{\hat{L},\gamma(IJ)} p_{\hat{L},\gamma(IJ)} - G_{\hat{R},\gamma(IJ)} p_{\hat{R},\gamma(IJ)} \right) \right) \tag{25}$$

where,

$$\kappa_{\hat{L},IJ} = w_{\hat{L},IJ} \left(\xi_{\hat{L},i(IJ)} + \xi_{\hat{L},j(IJ)} \right), \quad \kappa_{\hat{R},IJ} = w_{\hat{R},IJ} \left(\xi_{\hat{R},i(IJ)} + \xi_{\hat{R},j(IJ)} \right), \tag{26}$$

$$G_{\hat{L},\gamma(IJ)} = w_{\hat{L},IJ} \xi_{\hat{L},\gamma(IJ)} \quad \text{and} \quad G_{\hat{R},\gamma(IJ)} = w_{\hat{R},IJ} \xi_{\hat{R},\gamma(IJ)}, \quad \gamma = i, j \tag{27}$$

Using the harmonic points as interpolation points, we have built a new linear finite volume method with a multipoint flux approximation (MPFA). In Figure 2a, we show a typical interpolation stencil for the MPFA-H including the control volumes used to discretize the flux on the face IJ. We can note that this interpolation strategy includes only the immediate neighbors to construct the approximation. In contrast, the interpolation stencil in traditional MPFA methods (Fig. 2b) includes a larger number of control volumes to discretize the flux on the face IJ.
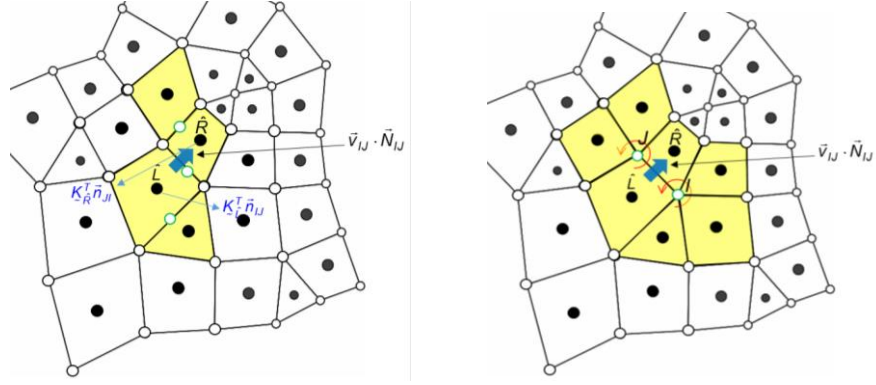
Figure 2. Stencil for the discret flux in the face using: (a) harmonic point as interpolation points and (b) typical MPFA method (e.g., MPFA-O).

3.3 Treatment of boundary fluxes

When the control surface (IJ) belongs to the contour $\Gamma_D \subset \mathcal{E}_{\hat{L}} \cap \mathcal{E}^{ext}$, the pressures are prescribed (Dirichlet boundary conditions) and the considering equation (15), as:

$$\vec{v}_{IJ} \cdot \vec{N}_{IJ} = \vec{v}_{IJ}^{\bar{L}} \cdot \vec{N}_{IJ} = \lambda_{IJ} \left\| \overrightarrow{IJ} \right\| k_{\hat{L},IJ} p_{\hat{L}} - \mathcal{G}_{\hat{L},IJ} \tag{28}$$

where $k_{\hat{L},IJ} = \xi_{\hat{L},i(IJ)} + \xi_{\hat{L},j(IJ)}$ and $\mathcal{G}_{\hat{L},IJ} = \xi_{\hat{L},i(IJ)} p_{\hat{L},i(IJ)} + \xi_{\hat{L},j(IJ)} p_{\hat{L},j(IJ)}$, and $p_{\hat{L},i(IJ)}$, $p_{\hat{L},j(IJ)}$ represent nodal pressures defined on Γ_D.

When the control surface (IJ) belongs to the contour $\Gamma_N \subset \mathcal{E}_{\hat{L}} \cap \mathcal{E}^{ext}$, the fluxes are imposed (Neumann boundary conditions) and again, considering equation (15), we can write:

$$\vec{v}_{IJ} \cdot \vec{N}_{IJ} = -g_N \left\| \overrightarrow{IJ} \right\| \tag{29}$$

In previous equation the specific flux on Γ_N is given by g_N.

3.4 Interpolation pressures on mesh faces

The definition and derivations of the interpolation points presented in this paper was originally proposed by (Agelas et al., 2009). Interpolation points over the control surfaces *IJ* of a particular CV, are obtained by

$$x_{IJ} = \frac{h_{\hat{L},IJ} k_{\hat{R},IJ}^{(n)} x_{\hat{R}} + h_{\hat{R},IJ} k_{\hat{L},IJ}^{(n)} x_{\hat{L}} + h_{\hat{L},IJ} h_{\hat{R},IJ} \left(\underset{\sim}{K}_{\hat{L}}^{\mathsf{T}} - \underset{\sim}{K}_{\hat{R}}^{\mathsf{T}} \right) \vec{n}_{IJ}}{h_{\hat{L},IJ} k_{\hat{R},IJ}^{(n)} + h_{\hat{L},IJ} k_{\hat{R},IJ}^{(n)}} \tag{30}$$

where $k_{\hat{L},IJ}^{(n)} = \vec{n}_{IJ}^{\mathsf{T}} \underset{\sim}{K}_{\hat{L}} \vec{n}_{IJ}$ and $k_{\hat{R},IJ}^{(n)} = \vec{n}_{IJ}^{\mathsf{T}} \underset{\sim}{K}_{\hat{R}} \vec{n}_{IJ}$ and $h_{\hat{L},IJ}$ (resp. $h_{\hat{R},IJ}$) denotes the ortogonal distance from $x_{\hat{L}}$ (resp. $x_{\hat{R}}$) to IJ. For control surfaces within the domain, i.e., $IJ \in \mathcal{E}^{\text{int}}$, if $x_{IJ} \in IJ$, the interpolation point given by equation (30) is called a harmonic point. For control surfaces that belong to the boundary, i.e., $IJ \in \mathcal{E}^{\text{ext}}$, we simply use the middle point of the edge as the interpolation point. When we are dealing with problems with high anisotropy or severely distorted meshes, the following cases can happen:

Case 1. Some harmonic average points may lay outside the mesh edges and the suummation of the angles $\theta_{\hat{L},IJ}^1 + \theta_{\hat{L},IJ}^2$ (see Fig. 3a) angles is greater than 180°. In this case, the harmonic points are calculated by the following equation:

$$x_{IJ} = \frac{h_{\hat{L},IJ} k_{\hat{R},IJ}^{(n)} x_{\hat{R}} + h_{\hat{R},IJ} k_{\hat{L},IJ}^{(n)} x_{\hat{L}}}{h_{\hat{L},IJ} k_{\hat{R},IJ}^{(n)} + h_{\hat{L},IJ} k_{\hat{R},IJ}^{(n)}} \tag{31}$$

Case 2. The harmonic average points still belong to the edge, even though the sum of angles $\theta_{\hat{L},IJ}^1 + \theta_{\hat{L},IJ}^2$ is greater than 180° (see Fig. 3b). In this case, the middle point replaces the harmonic point.

(a) (b)
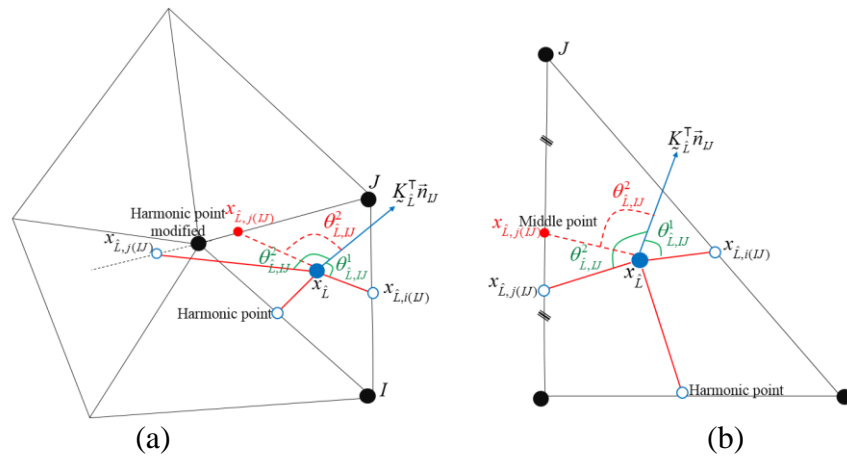
Figure 3. Representation of pathological cases: (a) harmonic average point that are localized outside edge and (b) harmonic average points over edges, but the sum the angles is greater than 180°.

The pressure in the interpolation point is calculated by the following convex combination:

$$p_{IJ} = w_{\hat{L},IJ} p_{\hat{L}} + w_{\hat{R},IJ} p_{\hat{R}} \tag{32}$$

where $w_{\hat{L},IJ}$ and $w_{\hat{R},IJ}$ defined in equation (21).

It is worth mentioning that the interpolation given in previous equations satisfies the linearity-preserving criterion, i. e., the truncation error vanishes in the linear case where the solution p is linear and the diffusion coefficient is constant on any cell $\hat{L} \in \mathcal{M}$.

3.5 The explicit saturation equation

In petroleum reservoir simulation, usually the advective term that characterize the hyperbolic saturation equation is discretized by the first order upwind (FOU) method which produces monote solutions by means of introducing a large amount of artificial diffusion (Peaceman 1977; Edwards 1996; Kozdon et al., 2011; Edwards 2006; Hirsch 2007). This method also strongly suffers grid orientation effects. On the other hand, the use of a strictly higher order scheme produces non-monotone solutions in the vicinity of regions with strong gradients in the saturation field (Contreras et al., 2016). In this context, it is of utmost importance to devise monotone, higher order and truly multidimensional formulations that can handle flows in non-homogeneous and non-isotropic porous media on general non-orthogonal polygonal unstructured meshes.

In the present paper, in order to discretize the saturation equation, we have adapted and implemented a second order finite volume method based on the MOOD strategy, which was originally proposed by Clain et al., (2011).

In order to obtain the discretized saturation equation, we first integrate equation (5) over an arbitrary control volume $\hat{L} \in \mathcal{M}$ with control surface $IJ \in \mathcal{E}_{\hat{L}}$ and use the divergence theorem of Gauss, yielding:

$$\int_{\hat{L}} \phi \frac{\partial S_w}{\partial t} dV = -\int_{IJ} \vec{F}(S_w) \cdot \vec{n} ds + \int_{\hat{L}} Q_w dV \tag{33}$$

For the sake of simplicity, we used the simple first order in time Euler forward method and obtain the following semidiscrete equation

$$S_{w,\hat{L}}^{m+1} = S_{w,\hat{L}}^m - \frac{\Delta t}{\phi V_{\hat{L}}} \left(\sum_{IJ \in \mathcal{E}_{\hat{L}}} \vec{F}_{IJ} \cdot \vec{N}_{IJ} - \bar{Q}_w V_{\hat{L}} \right) \quad \text{with} \quad \bar{Q}_w = \frac{1}{V_{\hat{L}}} \int_{\hat{L}} Q_w dV \tag{34}$$

where $\vec{F}_{IJ} \cdot \vec{N}_{IJ}$ is the numerical flux, and the superscripts *m* and *(m+1)* denotes physical quantities existing at instants t^m and t^{m+1}, respectively, and $\Delta t = t^{m+1} - t^m$ is the time step.

To approximate the numerical flux, we use the scheme proposed by (Serna 2009) and adapted in the context of reservoir simulation by (Souza, 2015):

$$\vec{F}_{IJ} \cdot \vec{N}_{IJ} = \begin{cases} \vec{F}_{IJ}^{LLF} \cdot \vec{N}_{IJ}, & \begin{cases} \dfrac{\partial f_w}{\partial S_w}\left(\tilde{S}_{w,IJ(\hat{L})}\right) \dfrac{\partial f_w}{\partial S_w}\left(\tilde{S}_{w,IJ(\hat{R})}\right) < 0 \quad \text{or} \\ \\ \dfrac{\partial^2 f_w}{\partial S_w^2}\left(\tilde{S}_{w,IJ(\hat{L})}\right) \dfrac{\partial^2 f_w}{\partial S_w^2}\left(\tilde{S}_{w,IJ(\hat{R})}\right) < 0 \end{cases} \\ \\ \vec{F}_{IJ}^{Up} \cdot \vec{N}_{IJ}, & \text{otherwise} \end{cases} \tag{35}$$

where f_w is the fractional flux function defined in equation (5), and $\tilde{S}_{w,IJ(\hat{L})}$ and $\tilde{S}_{w,IJ(\hat{R})}$ represent the higher order approximation for the saturation variable on face *IJ*, obtained from a polynomial reconstruction within control volumes $\hat{L}$ and $\hat{R}$, respectively.

In the equation (35) the upwind flux (LeVeque 1992) is given by:

$$\vec{F}_{IJ}^{Up} \cdot \vec{N}_{IJ} = \begin{cases} \vec{F}_{IJ}\left(\tilde{S}_{w,IJ(\hat{L})}\right) \cdot \vec{N}_{IJ}, & \text{if } \nu_{IJ} \geq 0 \\ \vec{F}_{IJ}\left(\tilde{S}_{w,IJ(\hat{R})}\right) \cdot \vec{N}_{IJ}, & \text{if } \nu_{IJ} < 0 \end{cases} \tag{36}$$

where the wave velocity on the face *IJ* is approximated by:

$$\nu_{IJ} = \frac{\partial \vec{F}_{IJ}}{\partial S_w} \cdot \vec{N}_{IJ} \tag{37}$$

To correct a possible violation of entropy, we use the Local Lax Friedrich (LLF) numerical flux, given, by:

$$\vec{F}_{IJ}^{LLF} \cdot \vec{N}_{IJ} = \frac{1}{2}\left(\left(\vec{F}_{IJ}\left(\tilde{S}_{w,IJ(\hat{L})}\right) + \vec{F}_{IJ}\left(\tilde{S}_{w,IJ(\hat{R})}\right)\right) \cdot \vec{N}_{IJ} - \max_{\hat{R},\hat{L}}\left|\nu_{IJ}\right|\left(\tilde{S}_{w,IJ(\hat{R})} - \tilde{S}_{w,IJ(\hat{L})}\right)\right) \tag{38}$$

where the term: $\max_{\hat{R},\hat{L}}\left|\nu_{IJ}\right|\left(\tilde{S}_{w,IJ(\hat{R})} - \tilde{S}_{w,IJ(\hat{L})}\right)$ corresponds to the artificial dissipation needed to stabilize the original central scheme.

3.6 Higher order finite volume and the MOOD strategy

The classical methods based in the MUSCL method of (van Leer 1979) use an *a priori* limitation procedure in order to reinforce monotonicity (Bell and Shubin 1985; Durlofsky 1993; Edwards 1996; Edwards 2006; Park et al., 2010; Contreras et al., 2016). On the other hand, in the MOOD procedure, higher order candidate solutions are first obtained by means of any robust formulation such as a gradient extrapolation or a discontinuous Galerkin method.

In order to obtain a second order approximation, we employ a piecewise linear reconstruction procedure (Edwards 1996; Edwards 2006; Hirsch 2007; van Leer 1979). Therefore, our upwind-biased linearly reconstructed saturations, $\tilde{S}_{w,IJ(\hat{L})}$ and $\tilde{S}_{w,IJ(\hat{R})}$, are computed as:

$$\tilde{S}_{w,IJ(\hat{L})} = S_{w,\hat{L}} + \frac{1}{4}\left[(1-\chi)\Delta_{\hat{L}}^- + (1+\chi)\left(S_{w,\hat{R}} - S_{w,\hat{L}}\right)\right] \tag{39}$$

$$\tilde{S}_{w,IJ(\hat{R})} = S_{w,\hat{R}} - \frac{1}{4}\left[(1-\chi)\Delta_{\hat{R}}^+ + (1+\chi)\left(S_{w,\hat{R}} - S_{w,\hat{L}}\right)\right] \tag{40}$$

Here χ represents a parameter used to control the degree of the approximation (Hirsch 2007; Blasek 2001; Lonher 2008). When one wants a high order approximation MUSCL-type, the second term in the equations (39) and (40) is premultiplicated by a limiter function.

Along the direction of the vector $\overrightarrow{\hat{L}\hat{R}}$ (Fig. 4) we define the difference operators, denoted by $\Delta_{\hat{L}}^{-}$ (upstream), $\Delta_{\hat{R}}^{+}$ (downstream), as:

$$\Delta_{\hat{L}}^{-} = S_{w,\hat{L}} - S_{w,\hat{L}^*} = 2\overrightarrow{\hat{L}\hat{R}} \cdot \nabla S_{w,\hat{L}} - \left(S_{w,\hat{R}} - S_{w,\hat{L}} \right) \tag{41}$$

$$\Delta_{\hat{R}}^{+} = S_{w,\hat{R}^*} - S_{w,\hat{R}} = 2\overrightarrow{\hat{L}\hat{R}} \cdot \nabla S_{w,\hat{R}} - \left(S_{w,\hat{R}} - S_{w,\hat{L}} \right) \tag{42}$$

where $\nabla S_{w,\hat{L}}$ and $\nabla S_{w,\hat{R}}$ denote the reconstructed gradients defined with respect to the left and right side control volumes, respectively. Following Blazek (Blasek 2001), the gradients are calculated by a least squares reconstruction. This reconstruction is based upon the use of a Taylor series expansion for each adjacent control volume connected to the cell $\hat{i}$.
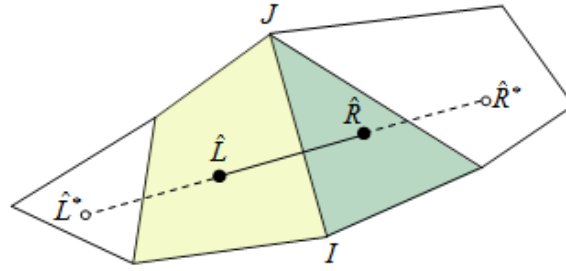
Figure 4. Stencil used to define the diference operators for the higher-order approximation, adapted from Contreras et al., (2016).

In this work, the MOOD scheme considers, initially, the maximum polynomial degree ($d_{max} = 2$) on each control volume to calculate the unlimited reconstruction on the face *IJ*, see equations (39) and (40). For a generic CV $\hat{L} \in \mathcal{M}$, the reconstructed values are used for the calculation of the numerical flux given in equation (35) in order to obtain the following candidate solution:

$$S_{w,\hat{L}}^{*} = S_{w,\hat{L}}^{m} - \frac{\Delta t}{\phi V_{\hat{L}}} \left(\sum_{IJ \in \mathcal{E}_{\hat{L}}} \vec{F}_{IJ}\left(\tilde{S}_{w,IJ(\hat{L})}\right) \cdot \vec{N}_{IJ} - \bar{Q}_w V_{\hat{L}} \right), \text{ for each } \hat{L} \in \mathcal{M} \tag{43}$$

where $\tilde{S}_{w,IJ(\hat{L})}$ represent the unlimited reconstructed saturation value on the face *IJ*.

Through an iterative decremental procedure, we determine the optimal degree $d_{\hat{L}} \leq d_{max}$, for each $\hat{L} \in \mathcal{M}$ when the candidate solution $S_{w,\hat{L}}^{*}$ satisfies the DMP criterion for any $\hat{k} \in \Lambda(\hat{L})$, so as:

$$\min_{\hat{k} \in \Lambda(\hat{L})} \left(S_{w,\hat{L}}^{m}, S_{w,\hat{k}}^{m} \right) \leq S_{w,\hat{L}}^{*} \leq \max_{\hat{k} \in \Lambda(\hat{L})} \left(S_{w,\hat{L}}^{m}, S_{w,\hat{k}}^{m} \right), \text{ for each } \hat{L} \in \mathcal{M} \tag{44}$$

where $\Lambda(\hat{L})$ represent the set of all control volumes that are immediate neighbors to $\hat{L}$.

The MOOD strategy can be summarized as (Clain et al., 2011):

1. Cell polynomial degree initialization $d_{\hat{L}} = d_{\max}$ for each $\hat{L} \in \mathcal{M}$.

2. Face polynomial degree evaluation d_{IJ}, using the following criterion:

$$d_{IJ} = \begin{cases} \min\limits_{IJ \in \mathcal{E}_{\hat{L}} \cap \mathcal{E}_{\hat{R}}} \left(d_{\hat{L}}, d_{\hat{R}} \right) & \text{or} \\ \min\limits_{\hat{R} \in \Lambda(\hat{L})} \left(d_{\hat{L}}, d_{\hat{R}} \right) \end{cases}$$

3. Update the reconstructed values $\tilde{S}_{w,IJ(\hat{L})}$ and evaluate the physical admissible criterion to avoid negative reconstructed values, i.e., we set $\tilde{S}_{w,IJ(\hat{L})} = \max(\tilde{S}_{w,IJ(\hat{L})}, 0)$.

4. Update the candidate solution $S^*_{w,\hat{L}}$, for each $\hat{L} \in \mathcal{M}$, using the equation (43).

5. The polynomial degree is decremented $d_{\hat{L}} = \max\left(0, d_{\hat{L}} - 1\right)$, and the solution is recomputed following steps 2 to 5 until all the control volumes satisfy the DMP criterion (equation (44)). Then the iterative procedure stops and $S^{m+1}_{w,\hat{L}} = S^*_{w,\hat{L}}$, for all $\hat{L} \in \mathcal{M}$.

4   NUMERICAL RESULTS

First, in order to evaluate the accuracy of the MPFA-H method, we briefly define the following L_2-norms to evaluate the discretizations errors:

$$\varepsilon_2^p = \left(\sum_{\hat{L} \in \mathcal{M}} \left(\overline{p}_{\hat{L}} - p_{\hat{L}} \right) V_{\hat{L}} \Big/ \sum_{\hat{L} \in \mathcal{M}} V_{\hat{L}} \right)^{0.5} \text{ and } \varepsilon_2^{\mathcal{F}} = \left(\sum_{IJ \in \mathcal{E}} \left(\overline{\mathcal{F}}_{IJ} - \mathcal{F}_{IJ} \right) V_{IJ} \Big/ \sum_{IJ \in \mathcal{E}} V_{IJ} \right)^{0.5} \tag{45}$$

where $\overline{p}$ is the analytical pressure, $\overline{\mathcal{F}}_{IJ}$ the analytical velocity and V_{IJ} is a representative volume for that edge, more precisely, it is the sum of volume of the CVs sharing edge *IJ*. The numerical convergence rates $R_\gamma \left(\gamma = p, \mathcal{F} \right)$ are obtained by the following expression:

$$R_\gamma = \log\left(\varepsilon_\gamma(h_2) \Big/ \varepsilon_\gamma(h_1) \right) \Big/ \log\left(h_2 / h_1 \right) \tag{46}$$

where h_1 and h_2 denote the mesh sizes of the two successive meshes.

4.1   One-phase flow in a mild anisotropic reservoir

This problem was adapted from (Gao and Wu 2010), and represents a one phase flow in a unitary square that is discretized by a set of successively refined grids (see Fig. 5 a-b) with full Dirichlet boundary conditions that are obtained directly from the exact solution given below:

$$\bar{p}(x,y) = \frac{1}{2}\left[\frac{\sin((1-x)(1-y))}{\sin(1)} + (1-x)^3(1-y)^2\right] \text{ and } \underset{\sim}{K} = \begin{pmatrix} 1.5 & 0.5 \\ 0.5 & 1.5 \end{pmatrix} \tag{47}$$

where $\underset{\sim}{K}$ is a homogeneous permeability tensor.

(a) (b) (c)
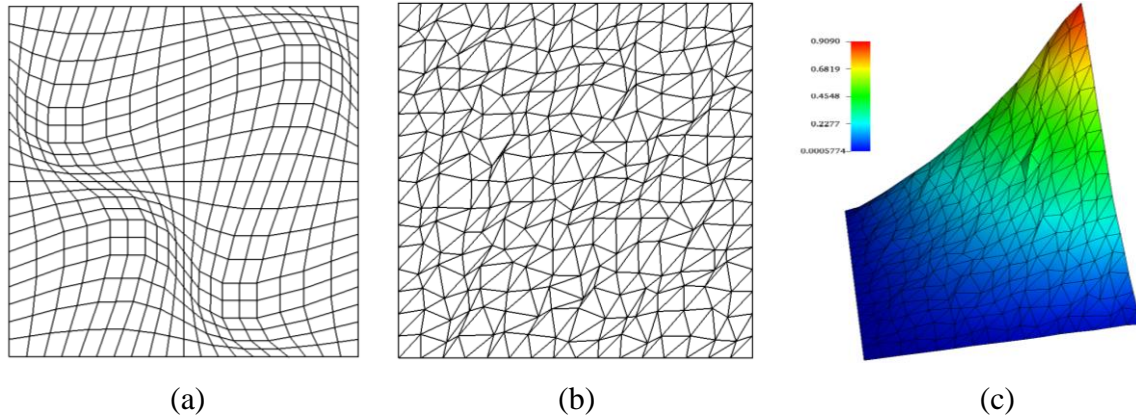
Figure 5. One-phase flow in a mild anisotropic reservoir: (a) distorted quadrilateral mesh, (b) randomly disturbed triangular mesh and (c) color map for pressure using triangular mesh

Errors and converegence rates can be seen in Tables 1 and 2. For this problem, the MPFA-H interpolation produces second order convergence rates for the scalar variable p and more than first order convergence rate for the fluxes. We perce that the method adopted is accurate and roboust even in structured quadrilateral mesh (Fig. 5-a) and slightly distorted mesh (Fig. 5-b), and in Fig. 5-c represents the solution profile obtained with the MPFA-H scheme on the coarse randomly disturbed mesh.

Table 1. Errors and convergence rates obtained with the distorted quadrilateral mesh using the MPFA-H for the one-phase flow problem in a mild anisotropic reservoir

Number of CVs	100	400	1600	6400
ε_2^p	0,0024	$6,5116 \times 10^{-4}$	$1,6620 \times 10^{-4}$	$4,1832 \times 10^{-5}$
R_p	----	1,8819	1,9701	1,9902
$\varepsilon_2^{\mathcal{F}}$	0,0190	0,0053	0,0014	$3,9751 \times 10^{-4}$
$R_{\mathcal{F}}$	----	1.8419	1.9205	1.8163

Table 2. Errors and convergence rates obtained with the randomly disturbed triangular mesh using the MPFA-H for the one-phase flow problem in a mild anisotropic reservoir

Number of CV	128	512	2048	8192
ε_2^p	$9,744 \times 10^{-4}$	$2,7377 \times 10^{-4}$	$5,8921 \times 10^{-5}$	$1,4929 \times 10^{-5}$
R_p	----	1,8315	2.22	1,9806
$\varepsilon_2^{\mathcal{F}}$	0,0176	0,0077	0,0032	0,0017
$R_{\mathcal{F}}$	----	1,1926	1,2697	0.908

4.2   1-D Buckley-Leverett problem

This classical problem, which was adapted from (Bastian 2014), consists in a 1-D oil-water displacement in a homogeneous reservoir that is originally filled with oil. We use this simple problem to appraise the relative accuracy and computational efficiency of the MOOD method versus the First Order Upwind (FOU) method and the two other higher order methods (HOMFV and HOFV-E) that were described in Contreras et al. (2016). Following Bastian (2014), who solved the saturation equation using a Discontinuous Galerkin (DG) method, we do not compute the pressure field, and the velocity field is set to $v = 10^{-7} \, m/s$, constant throughout the entire computational domain $\Omega = [0,300] \times [0,75][m]$. In this case, the irreducible water saturation (S_{irw}) and the residual oil saturation (S_{ro}) are given by $S_{irw} = S_{ro} = 0$ and the water saturation is prescribed at the left side of the reservoir, $\bar{S}_w^{inj} = 1$. The mobility ratio is $M \cong (\mu_o/\mu_w) = 1$, and we use a Corey-type relative permeability relation of the form $k_{rw}(S_w) = S_w^4$, and $k_{ro} = S_w^2 (1 - S_w^2)$. In this non-smooth problem, for which there is a semi analytical solution of (Bastian, 2014), we compute the errors in the saturation field using the L_1-norm, $\varepsilon_1^{S_w}$, given in the following equation using a target error of $\varepsilon_1^{S_w} < 4 \times 10^{-3}$.

$$\varepsilon_1^{S_w} = \sum_{\hat{L} \in \mathcal{M}} \left(\bar{S}_{w,\hat{L}} - S_{w,\hat{L}} \right) V_{\hat{L}} \Big/ \sum_{\hat{L} \in \mathcal{M}} V_{\hat{L}} \tag{48}$$

In the previous equation, $\bar{S}_{w,\hat{L}}$ and $S_{w,\hat{L}}$ are, respectively, the approximate and the exact values of the water saturation at a particular control volume $\hat{L} \in \mathcal{M}$. In Fig. 6, we present the saturation profiles for the methods. In table 3, we present the simulation times in seconds and errors in the L$_1$-norm for the four considered schemes. For this 1-D case, in order to approximately achieve the same accuracy of the higher order methods, the FOU method demands the use of a structured quadrilateral mesh with 512 control volumes along the horizontal axis while the higher order methods use a mesh with only 128 subdivisions, as it can be seen in table 3. In this table, we verify that the three higher order methods provide better accuracy than the FOU method at a lower computational cost. Besides, for this problem, the MOOD method has the biggest computational cost and it is slightly more accurate that the HOFV-E and the HOMFV methods.

Table 3. 1-D Buckley-Leverett problem: Errors in the *L*₁-norm and CPU times at t=1500 days

Method	*Mesh size along x-axis*	$\varepsilon_1^{S_w}$	*CPU Time (s)*
FOU	512x1	0.0026467	414.2655
HOFV-E	128x1	0.003394	137.5278
HOMFV	128x1	0.003621	165.5355
MOOD	128x1	0.002919	172.1796

(a)   (b)
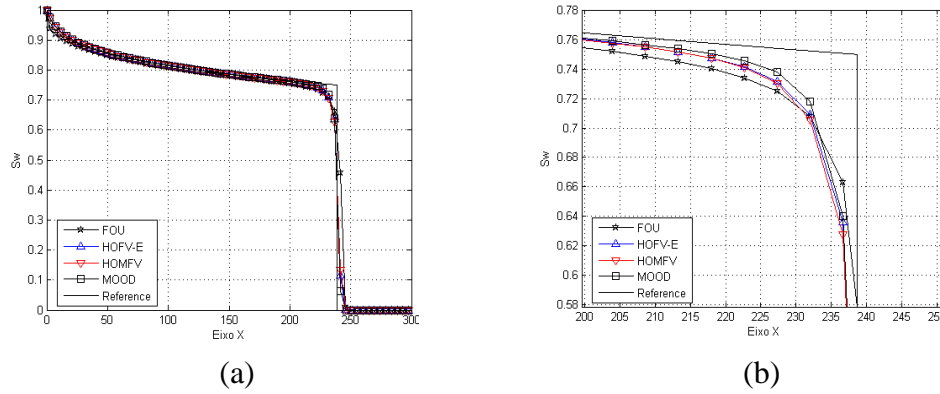
Figure 6. 1-D Buckley-Leveret Problem: (a) Saturation profiles obtained using first order and the higher order methods with 512 and 128 control volumes, respectively. (b) Zoom in the saturation shock region

4.3   Two-phase flow in a ¼ of five spot configuration in a homogeneous and anisotropic reservoir using a distorted triangular mesh

This example, adapted from (Lamine and Edwards 2010), consists in a variation of the classical ¼ of five spot problem, in which we use a full homogeneous permeability tensor with principal axes rotated 45 degrees in relation to the square domain, with an anisotropy ratio of $K_{xx}/K_{yy} = 10$. The oil and water viscosity ratio is $M \cong (\mu_o/\mu_w) = 1$, and the relation between the relative permeabilities is linear with $k_{rw} = S_w$ and $k_{ro} = 1 - S_w$. In this case, null flux boundary conditions are imposed at all external reservoir boundaries. The water flow rate prescribed at the injection well is $\bar{Q}_{inj} = 1$, and the pressure is prescribed at the producer with $\bar{p}_{prod} = 0$. For comparison purposes, we solve this problem using the MPFA-H scheme coupled to the MOOD, the FOU, the HOFV-E and the HOMFV methods. As a reference solution, we also use a more classical strategy, in which we solve the pressure field using MPFA-O method (Aavatsmark 2002) together with the FOU method using an unstructured and uniform quadrilateral mesh with 14988 control volumes, see Fig. 7-b. For all methods and mesh configurations, we used a CFL number of 0.4. According to (Lamine and Edwards 2010), an important feature of this example is the advective transport of a "stable" discontinuity throughout the domain. In Figure 7-c, it is clear that the higher order methods have much less numerical diffusion than that produced by the first order method. besides, the HOMFV and MOOD methods produce bounded solutions for the saturation equation, while the HOFV-E produce overshoots and unvershoots see Fig. 7-c.In Figure 8, we present the oil recovery and the cumulate oil curves for this problem. In these figures, we observe that the curves obtained by the MPFA-H coupled with the high-order methods are much closer to each other and to the reference solution than those obtained by the MPFA-H/FOU method.

(a) (b) (c)
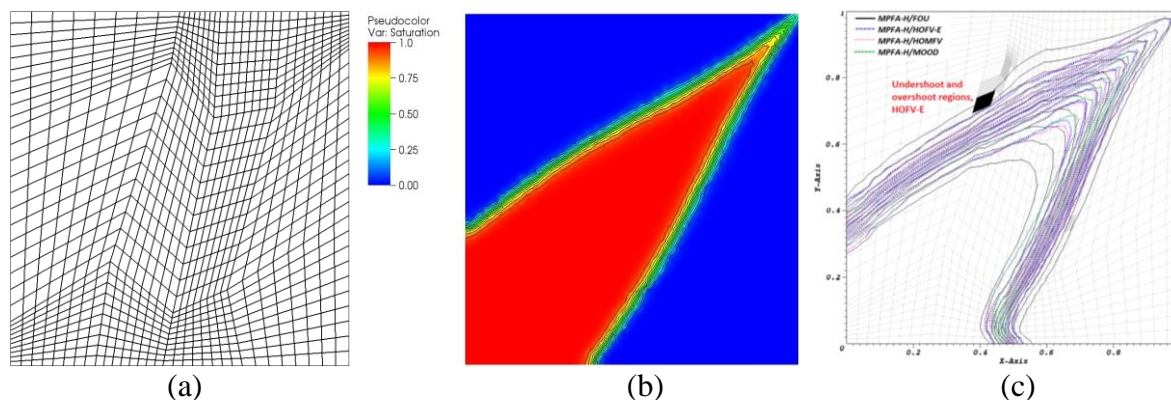
Figure 7. Two-phase flow in a ¼ of five spot configuration in a homogeneous and anisotropic reservoir: a) distorted quadrilateral mesh with 1024 control volumes; b) Reference solution at 0.4 PVI obtained with an unstructured uniform quadrilateral mesh with 14,988 control volumes; c) Saturation profiles obtained by the different methods (right)
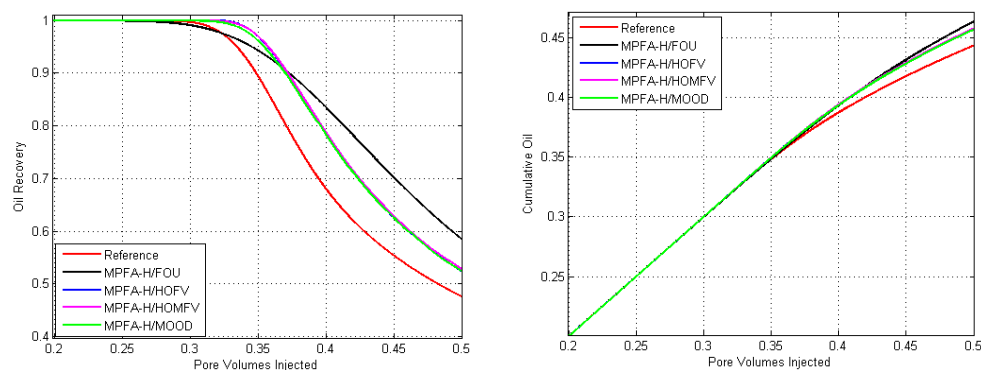
Figure 8. Results obtained for the ¼ of five spot problem in a homogeneous and anisotropic reservoir with a distorted quadrilateral mesh: recovered oil (left) and cumulative oil (right)

5 CONCLUSIONS

In this paper, we have described a cell-centered full finite volume method to simulate the displacement of oil by water in heterogeneous and anisotropic petroleum reservoirs. In order to discretize the elliptic pressure equation, we devised a linear multipoint flux approximation finite volume formulation that satisfies the linearity-preserving criterion using an interpolation based in harmonic points (MPFA-H). To discretize the hyperbolic saturation equation, we used the higher order MOOD method based in a least squares gradient reconstruction. In contrast with others classical finite volume methods, the MOOD strategy is based on an "*a posteriori*" limitation procedure in order to reinforce monotonicity. Three representative model examples were used to prove the effectivity of our formulation. In the near future, we intend to test our formulation in more chalenging problems, including highly heterogeneous and anisotropic reservoirs and flows with high mobility ratios.

ACKNOWLEDGEMENTS

REFERENCES

Aavatsmark, I., Barkve, T., Bøe, O., & Mannseth, T., 1998. Discretization on unstructured grids for inhomogeneous, anisotropic media. Part I: Derivation of the methods. *SIAM Journal on Scientific Computing* 19.5: 1700-1716.

Agelas, L., Eymard, R. & Herbin, R., 2009. A nine point finite volume scheme for the simulation of diffusion in heterogeneous media, *C.R. Acad. Sci. Paris Ser*, 347:673-676.

Bell, J. B., & Shubin, G. R., 1985. Higher-order Godunov methods for reducing numerical dispersion in reservoir simulation. *SPE Reservoir Simulation Symposium*. Society of Petroleum Engineers.

Bastian, P., 2014. A fully-coupled discontinuous Galerkin method for two-phase flow in porous media with discontinuous capillary pressure. *Computational Geosciences* 18.5: 779-796.

Blasek, J., 2001. *Computational Fluid Dynamics: Principles and Applications*. Elsevier.

Clain, S., Diot, S., & Loubere, R., 2011. A high-order finite volume method for systems of conservation laws Multi-dimensional Optimal Order Detection (MOOD). *Journal of computational Physics* 230.10: 4028-4050.

Colella, P., 1985. A direct Eulerian MUSCL scheme for gas dynamics. *SIAM Journal on Scientific and Statistical Computing* 6.1: 104-117.

Contreras, F. R. L., Lyra, P. R. M., Souza, M. R. A., & Carvalho, D. K. E., 2016. A cell-centered multipoint flux approximation method with a diamond stencil coupled with a higher order finite volume method for the simulation of oil–water displacements in heterogeneous and anisotropic petroleum reservoirs. *Computers & Fluids* 127: 1-16.

Carvalho, D. K. E., Willmerdorf, R. B. & Lyra, P. R. M., 2009. Some results on the accuracy of an edge-based finite volume formulation for the solution of elliptic problems in non-homogeneous and non-isotropic media. *International journal for numerical methods in fluids* 61.3: 237-254.

Carvalho, D. K. E., Willmersdorf, R. B. & Lyra, P. R. M., 2007. A node-centred finite volume formulation for the solution of two-phase flows in non-homogeneous porous media. *International journal for numerical methods in fluids* 53.8: 1197-1219.

Durlofsky, L. J., 1993. A triangle based mixed finite element finite volume technique for modeling two-phase flow through porous media. *Journal of Computational Physics* 105.2: 252-266.

Edwards, M. G., 1996. A higher-order Godunov scheme coupled with dynamic local grid refinement for flow in a porous medium. *Computer Methods in applied mechanics and engineering* 131.3: 287-308.

Edwards, M. G., & Clive, F. R., 1998. Finite volume discretization with imposed flux continuity for the general tensor pressure equation. *Computational Geosciences* 2.4: 259-290.

Edwards, M. G., 2006. Higher-resolution hyperbolic-coupled-elliptic flux-continuous CVD schemes on structured and unstructured grids in 2-D. *International journal for numerical methods in fluids* 51.9-10: 1059-1077.

Ewing, R. E., 1983. The mathematics of reservoir simulation. SIAM.

Fuhrmann, J., Ohlberger, M. & Rohde, C., 2014. *Finite Volumes for Complex Applications VII: Methods and Theoretical Aspects*.

Gao, Z. & Wu, J., 2010. A linearity-preserving cell-centered scheme for the heterogeneous and anisotropic diffusion equations on general meshes. *International Journal Numerical Method Fluids,* 67:2157-2183.

Gao, Z. & Wu, J., 2013. A small stencil and extremum-preserving scheme for anisotropic diffusion on arbitrary 2D and 3D meshes. *Journal of Computational Physics*, 250,308-331.

Hirsch, C., 2007. *Numerical computation of internal and external flows: The fundamentals of computational fluid dynamics*. Butterworth-Heinemann.

Kozdon, J. E., Mallison, B. T., & Gerritsen, M. G., 2011. Multidimensional upstream weighting for multiphase transport in porous media. *Computational Geosciences* 15.3: 399-419.

Lamine, S. & Edwards, M., 2010. Multidimensional upwind convection schemes for flow in porous media on structured and unstructured quadrilateral grids. *Journal of Computational and Applied Mathematics,* 234:2106-2117.

Le Potier, C., 2005. Schéma volumes finis monotone pour des opérateurs de diffusion fortement anisotropes sur des maillages de triangles non-structurés. *Comptes Rendus Mathématique* 341.12: 787-792.

LeVeque, R. J., & Leveque, R. J., 1992. *Numerical methods for conservation laws*. Vol. 132. Basel: Birkhäuser.

Lipnikov, K., Shashkov, M., Svyastskiy, D. & Vassilevski, Y., 2007. Monotone finite volume schemes for diffusion equations on unstructured triangular and shape-regular polygonal meshes. *Journal of Computational Physics*, 227(1):492-512.

Lönher, R., 2008. *Applied computational fluid dynamics techniques: an introduction based on finite element methods*. John Wiley & Sons.

Peaceman, D. W., 1977. *Fundamentals of Numerical Reservoir Simulation*. Elsevier, Amsterdam/New York.

Park, J. S., Sung-Hwan Y., & Kim, C., 2010. Multi-dimensional limiting process for hyperbolic conservation laws on unstructured grids. *Journal of Computational Physics* 229.3: 788-812.

Serna, S., 2009. A characteristic-based nonconvex entropy-fix upwind scheme for the ideal magnetohydrodynamic equations. *Journal of Computational Physics*, *228*(11), 4232-4247.

Souza, M. R. A., 2015. Simulação Numérica de Escoamento *Bifásico em reservatório de Petróleo Heterogêneos e Anisotrópicos utilizando um Método de Volumes Finitos "Verdadeiramente" Multidimensional com Aproximação de Alta Ordem* .Tese-UFPE, Brasil.

van Leer, B., 1979. Towards the ultimate conservative difference scheme. V. A second-order sequel to Godunov's method. *Journal of computational Physics* 32.1: 101-136.

Woodfield, P. L., Kenjiro, S. & Kazuyoshi, N., 2004. A simple strategy for constructing bounded convection schemes for unstructured grids. *International Journal Numerical Method Fluids*, 46:1007-1024.

Yuan, G. & Sheng, Z., 2008. Monotone finite volume schemes for diffusion equations on polygonal meshes. *Journal of computational physics* 227.12: 6288-6312.